Semina Ciências Exatas e Tecnológicas

e-ISSN 1679-0375
ENGINEERINGS

ORIGINAL ARTICLE DOI 10.5433/1679-0375.2024.v45.51520

Experimental Aerodynamics of a NACA 4424 Airfoil at Low Reynolds Number Flow

Aerodinâmica Experimental de um Aerofólio NACA 4424 em Escoaento de Baixo Número de Reynolds

Odenir de Almeida[1], Rafael de Rezende Dias[2]

Received: 28 September 2024 *Received in revised form: 18 November 2024* *Accepted: 28 November 2024* *Available online: 14 December 2024*

ABSTRACT

This paper presents wind tunnel data on the aerodynamic characteristics of a NACA4424 airfoil operating under low Reynolds number flow conditions ($\sim$ Re $= 2 \times 10^5$). The study investigates the lift, drag, and stall behavior of the airfoil, which are critical for applications in engineering such as small unmanned aerial vehicles (UAVs) and micro air vehicles (MAVs). Experimental data were collected through wind tunnel testing across various angles of attack at a fixed Reynolds number.To provide further insight, the experimental results are complemented by XFOIL simulations, which illustrate the impact of low Reynolds number conditions on aerodynamic performance. These findings enhance the understanding of airfoil behavior in low Reynolds number regimes and support the design and optimization of efficient airfoil profiles for small-scale aerial systems.

keywords NACA 4424, wind tunnel testing, low Reynolds flow, aerodynamics performance, small-scale aerial vehicle

RESUMO

Este artigo apresenta dados de túnel de vento sobre as características aerodinâmicas de um aerofólio NACA4424 operando em escoamento com baixo número de Reynolds ($\sim$ Re $= 2 \times 10^5$). O estudo se concentra nas características de sustentação, arrasto e estol do aerofólio, cruciais para várias aplicações de engenharia, como pequenos veículos aéreos não tripulados (UAVs) e micro veículos aéreos (MAVs). Dados experimentais foram obtidos por meio de testes em túnel de vento em vários ângulos de ataque para um número de Reynolds específico. A análise foi complementada por simulações XFOIL para destacar os efeitos do baixo número de Reynolds no desempenho aerodinâmico do aerofólio. As descobertas contribuem para a compreensão do comportamento aerodinâmico em números de Reynolds baixos, auxiliando no projeto e otimização de perfis de aerofólio para desempenho eficiente em sistemas aéreos de pequena escala.

palavras-chave NACA 4424, ensaios em túnel de vento, baixo número de Reynolds, desempenho aerodinâmico, micro-veículos aéreos

[1]Prof. Dr., Experimental Aerodynamics Research Center, UFU, Uberlândia, MG, Brazil. odenir.almeida@ufu.br
[2]Grad. Student, Experimental Aerodynamics Research Center, UFU, Uberlândia, MG, Brazil. rafaelrezendedias@ufu.br

Introduction

The aerodynamic performance of airfoils under low Reynolds number flow conditions is of significant interest in various engineering applications, particularly in the design and optimization of small unmanned aerial vehicles (UAVs) and micro air vehicles (MAVs). Understanding the behavior of airfoils at low Reynolds numbers is essential for achieving efficient and stable flight characteristics in these small-scale aerial systems.

As discussed by Winslow et al. (2018), most researchers have generally focused on $10^5 < \mathrm{Re} < 10^6$ as the low-Reynolds-number range. However, this range excludes further lower Reynolds numbers, that is, less than 105, which is of most interest to MAVs, UAVs, and low-speed flight designers. It is also known that simply trying to downsize conventional airfoils to low-Reynolds-number scales, drastically reduces their aerodynamic efficiency in terms of the lift-to-drag ratio (Mueller, 1985). At low Reynolds number flow, boundary layer developing over the airfoil may be subjected to laminar flow separation, transition to turbulence and reattachment. The appearing of a laminar-separation-bubble (LSB) will compromise the flow dynamics affecting the pressure distribution and the aerodynamics forces generated by the airfoil (Choudhry et al., 2015; Genç et al., 2016).

Traub and Coffman (2019) showed that the Re realm of micro aerial vehicles (MAVs) and small birds is typically between 10^4 and 10^5, whereas $\mathrm{Re} < 10^4$ is typically the domain of insects. Large birds, moderate-size unmanned aerial vehicles, and hobbyist radio-controlled aircraft often operate at $10^5 < \mathrm{Re} < 10^6$. Additionally, below 10^5 small changes in a Reynolds number have a much more prominent effect on airfoil performance than they would at a higher Reynolds number. Early, Schroeder and Baeder (2005) pointed out that computational fluid dynamics (CFD) can be used where experiments at low Reynolds number flow are difficult to perform well. Dongli et al. (2015) stated that the airfoil used for HAUAVs (high-altitude UAV) is usually designed in big maximum relative thickness for the sake of structural strength, which would bring with the loss of aerodynamic forces. Meanwhile the laminar separation bubble would change according to the variation of thickness, which affects the airfoil performance.

It is also known that, for MAV applications, commonly are employed cambered airfoils for better lift and symmetrical airfoils for maneuverability. Among the airfoil profiles studied for such applications is the NACA 4-digit series, renowned for its favorable lift and drag characteristics. For MAVs, thin and cambered variations, such as the NACA-2412, are adapted for low Reynolds number conditions (Bourisli & Hamadeh, 2020). Eppler airfoils are also often referenced for MAVs due to their good lift and drag characteristics in low-speed flight. Others applications are also found in literature such as the NACA-2205 (Marathe & Deshmukh, 2023), thinner airfoils such as AS6091 (Ananda & Selig, 2018) or even membrane airfoils such as Lian et al. (2003).

The use of thicker aifoils applied to MAV are scarce in literature. Despite the fact that thinner or cambered airfoils are generally preferred for maximizing aerodynamic efficiency in low-speed flight, thicker airfoils can be used in Micro-Air-Vehicles (MAVs) to provide structural strength, internal space for components, and improved lift at higher angles of attack. By considering this specific demands, this study focuses on the aerodynamics characterization of a thicker airfoil (NACA-4424) operating at low Reynolds number flow (2×10^5). The choice of NACA-4424 is also directed to the effect of airfoil thickness at low Reynolds number which involves a complex interplay between boundary layer pattern, stall characteristics, lift and drag coefficients, and aerodynamic efficiency. Understanding these effects is crucial for optimizing airfoil design for various low-speed applications, including small UAVs, MAVs, and other aerodynamic systems operating in similar flow regimes.

This paper presents a detailed analysis of wind tunnel data acquired for the NACA-4424 airfoil at low Reynolds number flow condition. This study was focused on the main aerodynamics characteristics such as lift, drag, pressure distribution and stall governing the performance of the NACA-4424 airfoil in regimes pertinent to small-scale aviation.

The airfoil was chosen due to its maximum relative thickness for the sake of structural strength, which would bring with the loss of aerodynamic forces. The effect of the thickness on the aerodynamics characteristics is extrapolated with XFOIL computational analyses. The experimental data gathered together with XFOIL analyses provide additional information for the design, optimization, and operation of aircraft operating within the realm of low Reynolds number aerodynamics.

The experimental apparatus used for this study are detailed in section Materials and methods, including the model geometry and wind tunnel setup, followed by a description of simple numerical approach by XFOIL. Both experimental and numerical data are compared in section Results and discussion, as well as the influence of the low Re effects on airfoil and its thickness. Concluding remarks are highlighted and future work are proposed as a continuation of this research in the realm of MAVs.

Materials and methods

Wind tunnel (TV-60)

The experiments were performed in a low speed wind tunnel (WT) at the Experimental Aerodynamics Laboratory (LAEX) at the Federal University of Uberlândia (UFU). The TV-60 Zephyr WT is used for academic and research purposes.

The test section has a cross section of 600 mm $\times$ 600 mm and 1000 mm in length, with maximum operational velocity of 26 m/s at the test section – Figure 1. It is equipped with a 25-horsepower electric motor which moves a 24-blade fan which blows the flow into an open-circuit well prepared with a set of guide-vanes and screens to control and guide the flow at the test section with low turbulence level (0.5 % at high speeds). The wind tunnel is equipped with a 3-component (lift, drag and moment) aerodynamic balance AA-TVAB1®, which is connected to a computer. Measurements are either software-processed or gathered directly in the aerodynamic digital display.

Figure 1 - The low speed wind tunnel (TV-60 Zephyr).

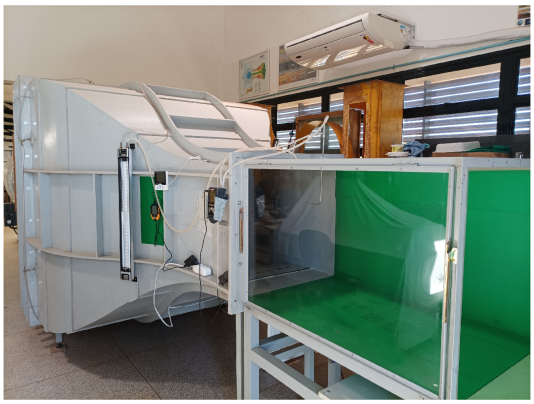

The flow velocity in the test section is measured using a L-type TPL-06-300 Pitot tube connected to a Kimo® MP200 digital manometer. For multiple pressure readings the tunnel can be equipped with analog pressure sensors (U-type water manometer) with 10 ports as well as digital pressure transducers, connected to an AA-TVCR2® with 64 channels pressure-module. Measurements of ambient conditions are gathered through a set of sensors for temperature and relative humidity - JIAXI® model HTC-2A and barometric pressure and altitude - SUNROAD® model Alt. All these equipment's were used in the different setups in this study, as described in the following sections.

Wind tunnel and aerodynamic balance calibration

A preliminary wind tunnel calibration was performed using the Pitot tube and pressure manometer MP200 as the reference instrument. Two curve fittings were then performed using Matlab® to post-process the current data.

The procedure consists of varying the electrical motor inverter frequency and reading the resultant flow velocity in the test section, true airspeed and differential pressure was indicated by the pressure manometer and should be recorded either digitally or manually. This apparatus has a declared accuracy of ± 0.5 % of reading ± 0.2 m/s for velocity values in the intended velocity range and ± 0.2 % or reading ± 0.8 Pa for values of pressure under 100 Pa and ± 0.2 % or reading ± 1.5 Pa for values above 100 Pa.

The resulting calibration shows a good linear relation between the input frequency and output test section airflow velocity as will be shown in the results section.

Later, a balance calibration was performed using a very thin steel cable and pulley system to impose the axial force (drag) and vertical force (lift) on the balance rod-connection. Also, a system with standard masses were used to simulate both lift and drag loads. Each measurement for lift and drag was performed 30 times in a set of 3 samples. The resulting calibration shows a good linear relation between the input and output mass and the results are illustrated in results section.

NACA-4424 test-article

The NACA-4424 airfoil was prepared for experiments covering lift, drag and pressure distribution. The test-article was printed in three separated pieces using a 3D printer (Makerbot® Replicator Z18). Subsequently, the three parts were bounded together and went through a surface finishing process, aiming to reduce possible roughness that could compromise the airfoil's aerodynamics characteristics.

The profile dimensions are respectively, chord = 250 mm, span = 565.2 mm and planform area = 141300 mm^2. Figure 2(a) highlights the 2D view of the aerodynamic profile while Figure 2(b) shows the final test-article instrumented with aerodynamic balance rod and pressure taps and hoses.

Figure 2 - (a) Airfoil NACA 4424 profile, (b) Finished model.

(a)

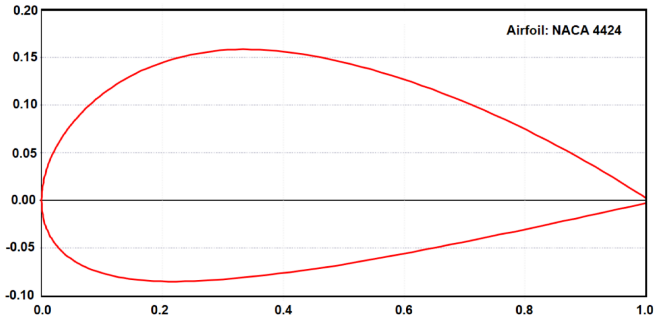

(b)

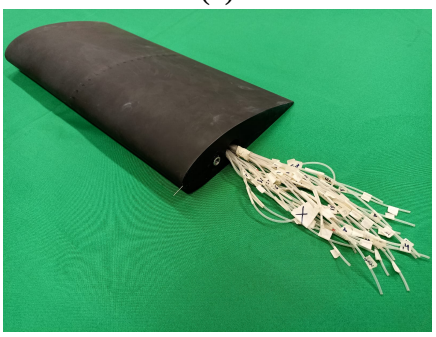

Wind tunnel setup

To acquire the values of the airfoil's lift (L) and drag forces (D), the NACA-4424 model was attached to a three-axis aerodynamic balance (AATVAB1®). To bring the model lift and drag coefficients closer to a 2D airfoil (infinite wing), splitter plates were used on both sides (at extremities), close enough to the test model to reduce the wingtip vortices by creating a physical barrier at the ends, but allowing the free movement of the model and not compromising the aerodynamic balance data acquisition. The lift and drag coefficients are given by equations (1) and (2):

$$c_l = \frac{L}{\frac{1}{2}\rho V_\infty^2 S}, \tag{1}$$

$$c_d = \frac{D}{\frac{1}{2}\rho V_\infty^2 S}, \tag{2}$$

respectively, ρ is the air density (kg/m^3), V_∞ is the freestream flow velocity (m/s), and S is the reference area (m^2).

Figure 3 shows the assembly of the experimental apparatus.

Figure 3 - (a) Airfoil lift and drag experiment schematics and (b) Airfoil assembled in the WT.

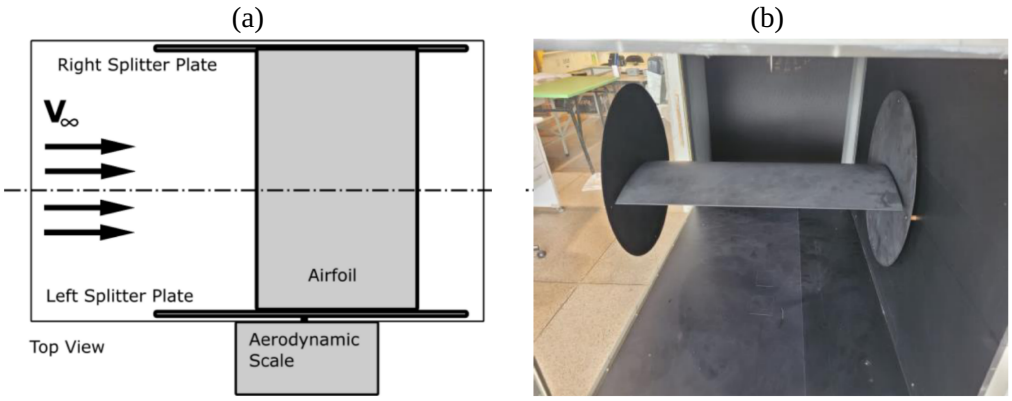

The test was performing varying the geometric angle of attack (AoA) of the airfoil in 1º per run according to the digital degree meter in the aerodynamic balance up to the stall condition, which is identified in the c_l vs AoA curve due to the reduction of the lift coefficient due to an excessive AoA, causing airflow separation on the upper side of the airfoil. For each test run, 10 measurements of lift (L) and drag (D) were taken. The experiment was performed for a Reynolds number of 2×10^5, according to equation (3):

$$Re = \frac{\rho V_\infty c}{\mu}, \tag{3}$$

where μ is the air dynamic viscosity (Pa.s) and c is the airfoil chord (m).

For the pressure distribution experiment, the NACA-4424 was equipped with 35 pressure ports (taps) connected to the AATVCR2® with a 64 pressure-transducer module.

Figure 4 shows the experiment schematic and real assembly in the wind tunnel.

Figure 4 - (a) Airfoil pressure experiment – schematic and, (b) Real model in the WT.

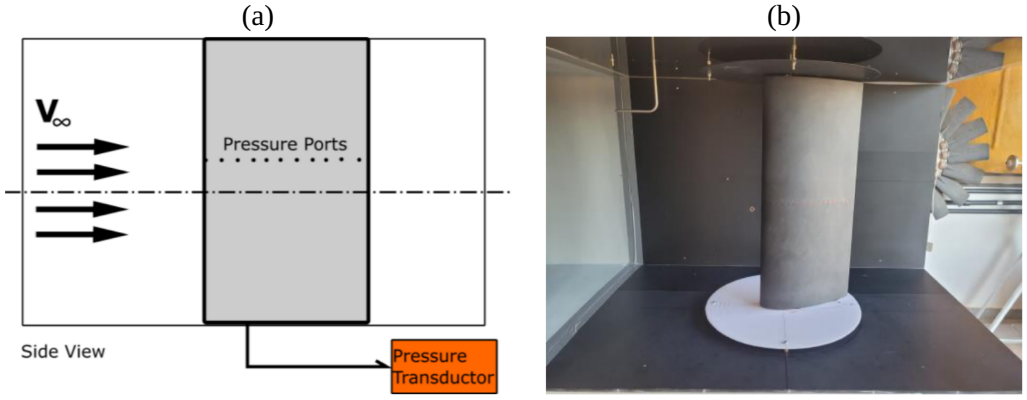

The only difference is that this model was assembled in the vertical position in the test section to facilitate the pressure cabling and connection to the pressure transducer module, that was placed underneath. For cable management reasons, the spatial distribution of pressure ports and its respective pressure channels were organized in the following way: pressure ports of numbers 1 up to 18 were placed in the upper surface of the airfoil with operational limit varying from 2 kPa up to 50 kPa due to resolution of the available channels in the pressure transducer; pressure ports of numbers 19 up to 35 were placed in the lower surface with operational limit varying from 10 kPa up to 50 kPa. The pressure coefficient was calculated by equation (4):

$$C_p = \frac{p - p_\infty}{\frac{1}{2}\rho V_\infty^2}, \tag{4}$$

where p is the static pressure (Pa), p_∞ is the ambient pressure (Pa).

XFOIL analysis

A complementary analysis was performed using XFOIL (Drela, 1989) with two purposes. The first, was to compare the numerical data with the experimental measurements for lift, drag and pressure distribution. The second purpose, was to extrapolate the analysis to verify the influence the airfoil thickness (t/c) in the lift coefficient (c_l) and drag coefficient (c_d) values.

XFOIL's viscous mode is enabled to account for the low Reynolds number effects by issuing the "visc" command. Finally, the analysis is run to calculate key aerodynamic parameters, such as lift coefficient (c_l), drag coefficient (c_d), and moment coefficient (c_m), for the specified conditions, and the results are reviewed or exported for further study.

The procedure is repeated for evaluating different airfoil thickness (t/c) from 10 up to 24 % in the NACA-4 digit airfoil's family – Figure 5.

Figure 5 - Complementary analysis with XFOIL to evaluate the influence of (t/c).

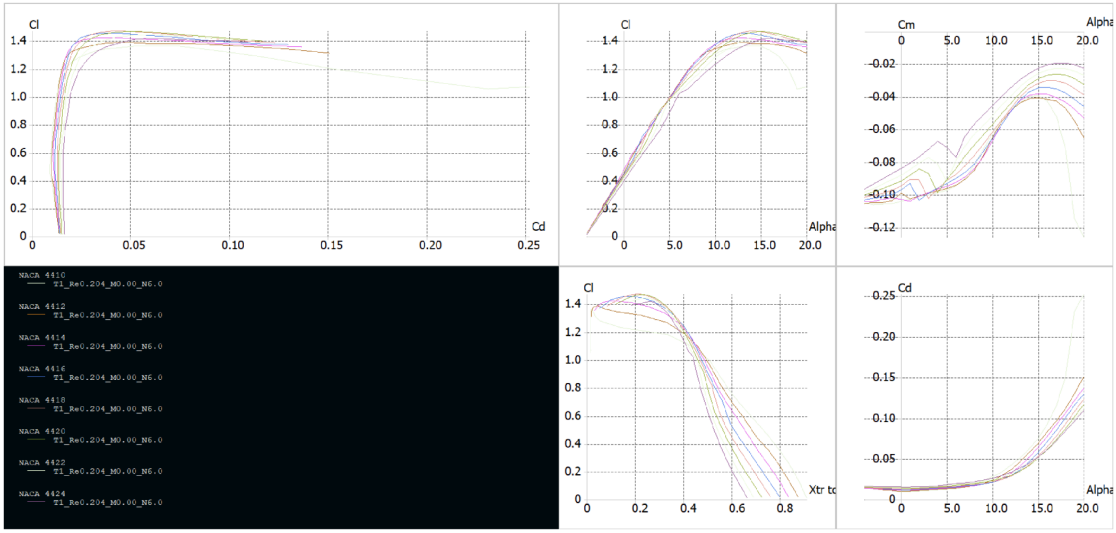

Results and discussion

Calibration data

The calibration curves for the wind tunnel and for the aerodynamic balance are seen in Figure 6 and Figure 7, respectively.

Figure 6 - TV-60 Zephyr calibration data (T = 26 ºC): (a) Velocity as function of frequency and (b) Velocity as function of DP.

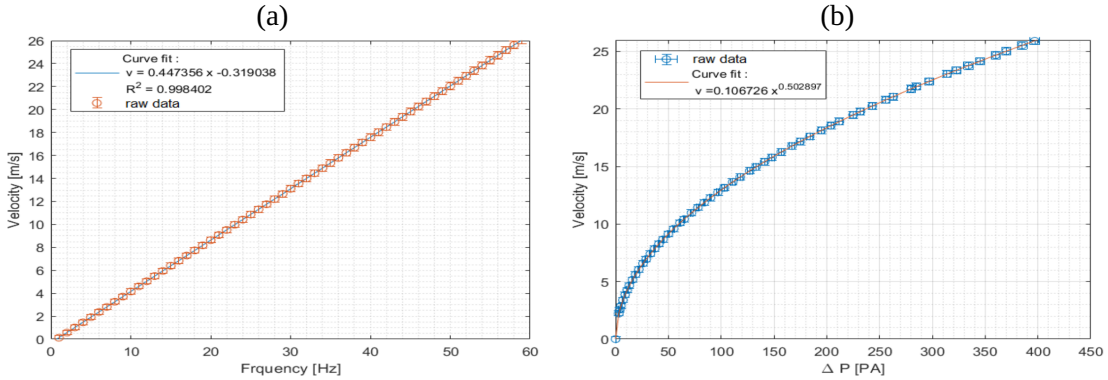

Figure 7 - Calibration curves (T = 24 ºC): (a) Lift and (b) Drag.

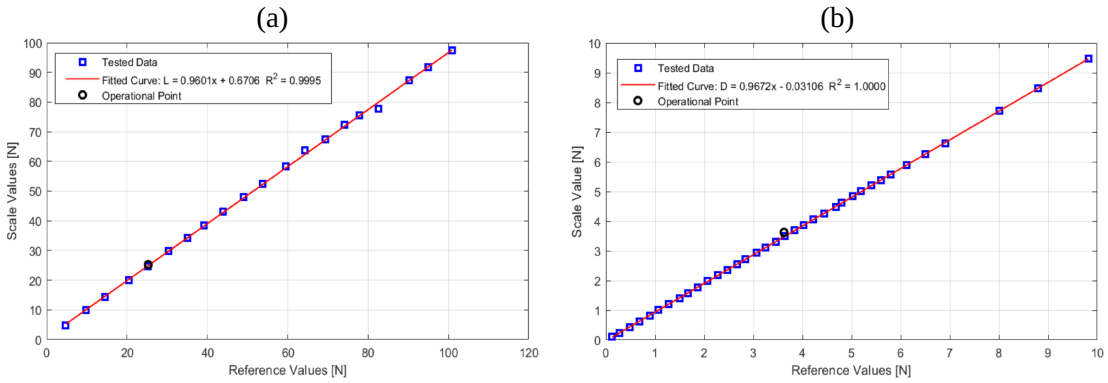

The WT calibration plot shows a good linear relation between the input frequency on the electrical motor and output airflow velocity in test section measured by the Pitot tube (R^2 = 0.998) as expected, assuring the right dynamic pressure upstream the model, see Figure 6. Also, the calibration curves for lift and drag were very consistent and give a linear relationship between the input load and output measured value ($0.999 < R^2 < 1.000$). In Figure 7 it is illustrated mid-range operational point for both curves (lift and drag) expected during the measurements.

Lift and drag coefficients

Figure 8 shows the results for lift coefficient (c_l) and drag coefficient (c_d) at a Reynolds number of 2×10^5 as function of the angle of attack (AoA) or α as well as the data obtained from XFOIL for comparison purposes.

Figure 8 - Airfoil lift and drag coefficients curves: (a) Lift vs AoA and (b) Drag vs AoA.

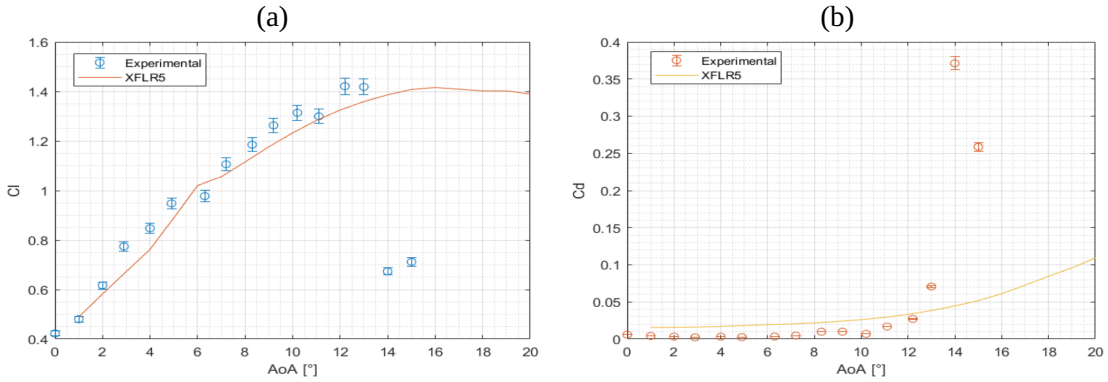

The experimental results show satisfactory consistency with low-speed airfoil theory and XFOIL data for low angles of attack, presenting a well-behaved $c_l \times \alpha$ and $c_d \times \alpha$ polars. However, at higher AoA (above 12º) some discrepancy is seen against XFOIL data. This is expected to happen due to the low Re number of the experiment where viscous effects play important role on the flow pattern what dictates the arfoil's aerodynamics characteristics. The airfoil stalls at around 14º and the maximum lift coefficient is 1.41, at which the climbing in the drag polar occurs (Anderson, 2011). In this setup, it was not possible to investigate the flow pattern around the airfoil by means of flow visualization techniques. As identified by other authors such as Genç et al. (2016), a laminar-separation-bubble (LSB) may be present close to the leading edge at this flow regime what could induce rapid loss of lift (stall condition).

C_p distribution

Figures 9 and 10 depicts the averaged pressure coefficient curves (C_p) for each angle of attack, as well as the correspondent XFOIL results, for comparison purposes. The results were consistent showing good pattern in the (C_p) distribution over upper and lower surfaces of the airfoil. The pressure port 26, located in the lower

surface of the airfoil presented wrong data with high standard deviation and it was dismissed. Later, it was concluded that this port had problem's connection with the pressure transducer.

Figure 9 - Pressure coefficient (C_p) results for AoA (α): (a) 0º, (b) 2º, (c) 4º and (d) 6º.

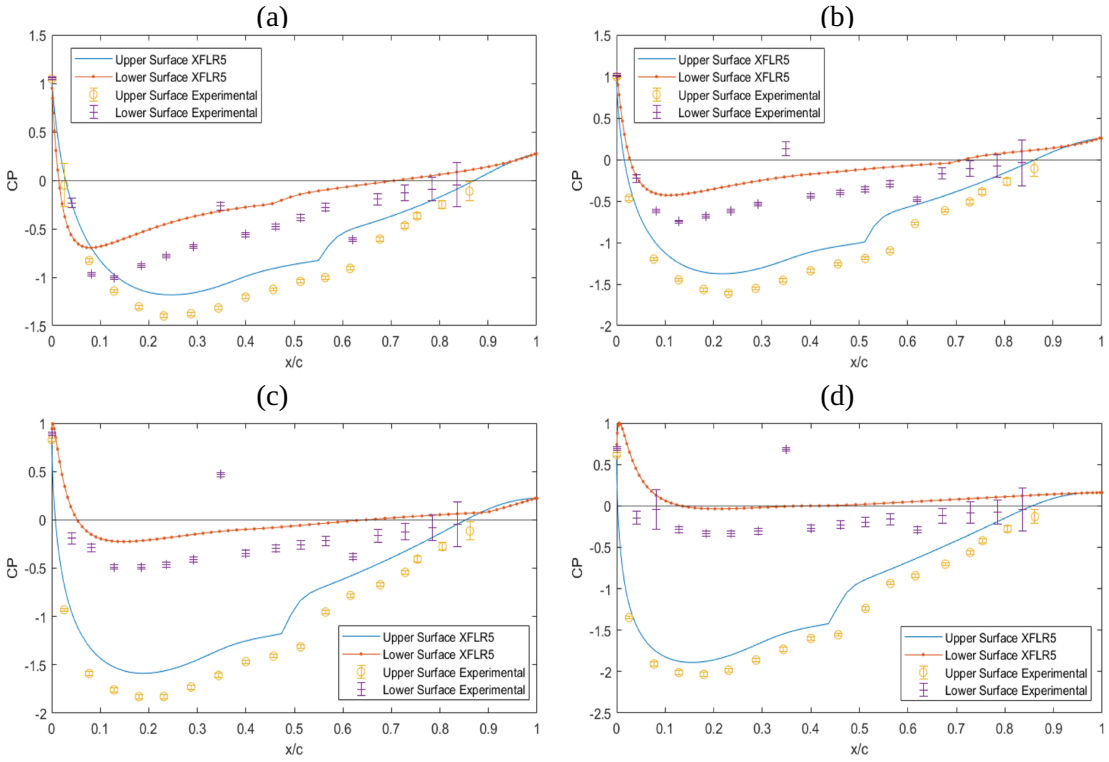

Figure 10 - Pressure coefficient (C_p) results for AoA (α):(a) 8º, (b) 10º, (c) 12º and (d) 14º.

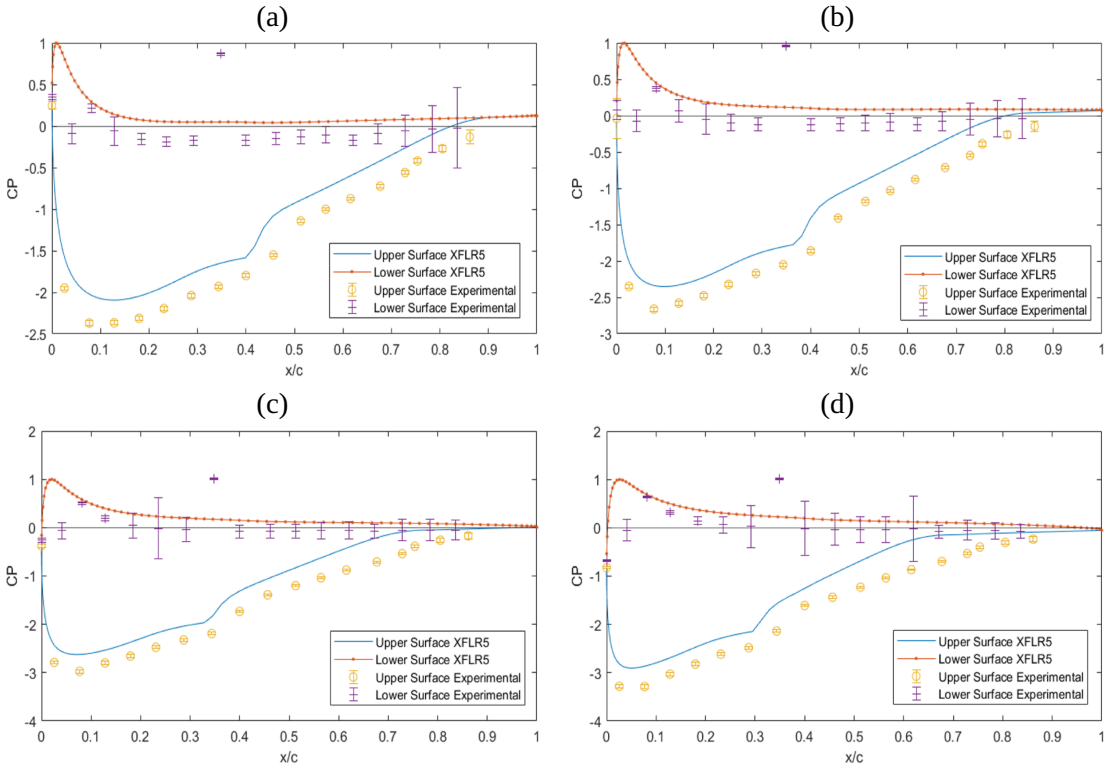

By inspecting the (C_p), Figures 9 and 10, distribution it is possible to observe the presence of a plateau and kink in the upper side of the airfoil indicating a laminar separation bubble (LSB), transition and reattachment. This trend was captured for all angles investigated from 2º up to 14º. Notably, as the α is increased above 4º the separation bubble starts to move upstream closer to the leading edge of the airfoil. The work of Choudhry et al. (2015) discuss the appearing of a long separation bubble (LoSBs) on thick airfoils and its consequences to the aerodynamics performance.

Airfoil thickness effect (XFOIL)

Figure 11 depicts the influence of the airfoil thickness (t/c) in the lift production (c_l). The analysis was performed with XFOIL by considering variations of the NACA-44XX, where XX represents the two-digits for the airfoil thickness, which varied from 10 up to 24 (NACA-4410 up to NACA-4424). The maximum lift was obtained for the NACA-4418 whose value is 1.469. The variation in percentage of Δc_l was of order -0.3 % for NACA-4420 up to -7.2 % for NACA-4410. The NACA-4424 airfoil presents a drop in the maximum c_l of order -3.7 %.

Figure 11 - Influence of airfoil thickness (t/c) in the lift coefficient (c_l).

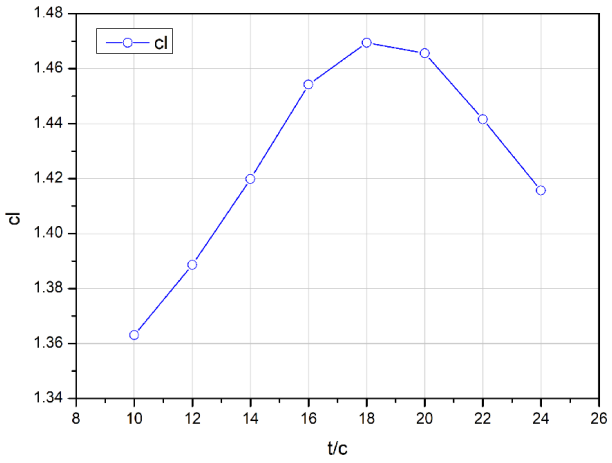

Conclusions

This work presented an experimental study, via wind tunnel tests, of the NACA 4424 airfoil at low Reynolds numbers (2×10^5) looking for the determination of its aerodynamic viability for low-speed applications such as micro-air-vehicles (MAVs). The main observations and outcomes are summarized as:

- The airfoil exhibited favorable lift-to-drag ratios, with predictable stall behavior and flow separation patterns while keeping a high value for the thickness that could be useful for structural purposes and fitting of onboard instruments/equipment.
- Through the analysis of the acquired data, it was possible to identify specific flow phenomena happening at this low Re regime, such as the appearance of laminar separation and formation of a laminar-separation-bubble. Despite the influence of the LSB in the airfoil performance, the c_l and cd data are still in the range of applicability for small aerial vehicles.
- The use of simple airfoil analysis through XFOIL allowed to check the experimental data as well as to extrapolate the verification for identifying the influence of the airfoil thickness. The NACA-4424 airfoil has a decrement of 3.7 % in percentage of Δc_l, when compared to best performance in terms of airfoil thickness (t/c) of NACA-4418.

Based on these findings, it is possible to affirm the potential for use of NACA-4424 in small-scale aircraft and UAVs, where efficient performance at low speeds is critical. Future studies could focus on optimizing the airfoil's design for specific low-speed flight conditions while keeping its benefits of thickness.

Author contributions

O. Almeida participated in: conceptualization, investigation, methodology, supervision, writing – revision and editing. R. R. Dias participated in: data curation, formal analysis, investigation, methodology, validation, writing-revision.

Conflicts of interest

The authors declare no conflict of interest.

Acknowledgments

The authors would like to thank the Financiadora de Estudos e Projetos (FINEP - 0138/11) for funding the CPAERO (Experimental Aerodynamics Research Center) from Federal University of Uberlândia (UFU).

References

Ananda, G. K., & Selig, M. S. (2018). Design of bird-like airfoils. In American Institute of Aeronautics and Astronautics, *AIAA Aerospace Sciences Meeting* [Proceedings]. AIAA Aerospace Sciences Meeting, Kissimmee, Florida. https://doi.org/10.2514/6.2018-0310

Anderson, J. (2011). *Fundamentals of Aerodynamics*. McGraw Hill.

Bourisli, R. I., & Hamadeh, F. Z. (2020). Optimizing NACA Airfoil Thickness Function Parameters for Maximum Lift-to-Drag Ratio. In American Institute of Aeronautics and Astronautics, *AIAA Scitech 2020 Forum* [Proceedings]. AIAA Scitech 2020 Forum, Orlando, Florida. https://doi.org/10.2514/6.2020-1297

Choudhry, A., Arjomandi, M., & Kelso, R. (2015). A study of long separation bubble on thick airfoils and its consequent effects. *International Journal of Heat and Fluid Flow*, *52*, 84–96. https://doi.org/10.1016/j.ijheatfluidflow.2014.12.001

Dongli, M., Yanping, Z., Yuhang, Q., & Guanxiong, L. (2015). Effects of relative thickness on aerodynamic characteristics of airfoil at a low Reynolds number. *Chinese Journal of Aeronautics*, *28*(4), 1003–1015. https://doi.org/10.1016/J.CJA.2015.05.012

Drela, M. (1989). XFOIL: An analysis and design system for low Reynolds number airfoils. In T. J. Mueller (Ed.), *Low Reynolds Number Aerodynamics. Lecture Notes in Engineering* (Vol. 54, pp. 1-12). Springer. https://doi.org/10.1007/978-3-642-84010-4_1

Genç, M. S., Koca, K., Açıkel, H. H., Özkan, G., Kırış, M. S., & Yıldız, R. (2016). Flow characteristics over NACA4412 airfoil at low Reynolds number. *EPJ Web of Conferences*, *114*, 1–5. https://doi.org/10.1051/epjconf/201611402029

Lian, Y., Shyy, W., Viieru, D., & Zhang, B. (2003). Membrane wing aerodynamics for micro air vehicles. *Progress in Aerospace Sciences*, *39*, 425–465. https://doi.org/10.1016/S0376-0421(03)00076-9

Marathe, M., & Deshmukh, S. (2023). Comparative Analysis Of Airfoil Selection For Miniature Air Vehicle. *International Journal of Engineering Applied Sciences and Technology*, *8*(2), 154–159. https://doi.org/10.33564/ijeast.2023.v08i02.021

Mueller, T. J. (1985). The influence of laminar separation and transition on low Reynolds number airfoil hysteresis. *Journal of Aircraft*, *22*(9), 763–770. https://doi.org/10.2514/3.45199

Schroeder, E., & Baeder, J. (2005). Using computational fluid dynamics for micro-Air vehicle airfoil validation and prediction. In American Institute of Aeronautics and Astronautics, *AIAA applied aerodynamics conference* [Proceedings]. 23rd AIAA applied aerodynamics conference, Toronto, Canada. https://doi.org/10.2514/6.2005-4841

Traub, L. W., & Coffman, C. (2019). Efficient low-Reynolds-number airfoils. *Journal of Aircraft*, *56*(5), 1987–2003. https://doi.org/10.2514/1.C035515

Winslow, J., Otsuka, H., Govindarajan, B., & Chopra, I. (2018). Basic understanding of airfoil characteristics at low Reynolds numbers (10^4–10^5). *Journal of Aircraft*, *55*(3), 1050–1061. https://doi.org/10.2514/1.C034415